Accelerated autofocusing of off-axis holograms using critical sampling

M. Fatih Toy,[1,*] Jonas Kühn,[1] Stéphane Richard,[2] Jérôme Parent,[1] Marcel Egli,[2] and Christian Depeursinge[1]

[1]*Microvision and Microdiagnostics Group (SCI STI CHD), École Polytechnique Fédérale de Lausanne (EPFL), Lausanne, CH-1015, Switzerland*

[2]*Space Biology Group, Eidgenössische Technische Hochschul (ETH) Zürich, Zürich, CH-8005, Switzerland*

**Corresponding author: fatih.toy@epfl.ch*

Received September 12, 2012; revised November 5, 2012; accepted November 8, 2012;
posted November 8, 2012 (Doc. ID 174499); published December 6, 2012

In this Letter we propose a fast off-axis hologram autofocusing (AF) approach that is based on the redundant data elimination by the critical resampling of the contained complex field. Implementation of the proposed methodology enables the real-time AF with up to 12× speed-up factors in comparison to the classical approach. The method is further extended for single-shot physical autofocus of the fluorescence imaging channel of multimodal imaging instruments capable of off-axis hologram acquisition.

OCIS codes: (090.1995) Digital holography, (090.2880) Holographic interferometry, (090.5694) Real-time holography, (110.0180) Microscopy, (180.2520) Fluorescence microscopy.

Digital holography (DH) enables the simultaneous recording of amplitude and phase field components, which are scattered by an object, on a digital camera [1]. Recorded digital holograms are numerically processed on demand to decode the complex wave field and numerically propagate it. Based on the physical configuration of the recording setup, the holograms are called either inline [2] or off axis [3]. DH, as an imaging modality, has recently received increased attention mainly due to ease of use of the technique and promising quantitative phase imaging.

In particular, digital holographic microscopy (DHM) has proven its potential as a label-free, fast, and noninvasive biomicroscopy method [4]. Besides, multimodal microscopes capable of DH and epifluorescence imaging were also developed [5,6]. Numerical focusing by the propagation of a reconstructed complex field is an intrinsic advantage of DHM, leaving the precise physical focusing redundant and unnecessary.

In this Letter, we present an accelerated autofocusing (AF) approach for off-axis holograms. The presented AF approach takes advantage of the sampling conditions of the recorded off-axis hologram by resampling the complex wave field. Performance gain in practical cases is given for experimental holograms. This AF approach is also exploited for the real-time DHM-fed physical refocus of a DH-fluorescence multimodal microscope. The DHM-fed physical refocus is used to keep live cell samples in focus in the epifluorescence imaging channel under drifting focus conditions. In this specific case, a microscope is used for live cell experiments in a parabolic flight campaign, during which alternating microgravity and hypergravity are experienced in the plane cabin, causing intermittent mechanical disturbances on the microscope.

In inline hologram recording, collinearly impending reference (R) and object (O) wave fields form the hologram in off-axis hologram recording whereas an angle exists between the two giving rise to a carrier signal (s_c) around where the Fourier spectral information of the object wave field is centered.

First, we only focus on the camera sampling and discrete Fourier transformation conditions. Pixel count and two-dimensional (2D) orientation of the recording device introduce hard limits on the maximal size of discrete Fourier spectral support of the object wave field ($s_o^{\max}$) allowed for nonaliased content of off-axis holograms as shown in Fig. 1.

On a planar recording device, the limit, $s_o^{\max}$, varies with the 2D orientation of s_c and has two extremities, when s_c is on a principle axis or when on a diagonal orientation as given in Eq. (1):

$$s_O^{\max} \le \frac{N}{4} \text{ when } (s_c(u,0) \neq 0 \vee s_c(0,v) \neq 0)$$
$$s_O^{\max} \le \frac{2N}{2+3\sqrt{2}} \text{ when } (s_c(u,u) \neq 0). \quad (1)$$

In the equation, N is the number of pixels in one direction for both hologram and its spectrum and u and v correspond to discrete spatial frequencies on axes x and y.

Now we consider the influence of a microscope objective (MO) of a DHM positioned before the recording device. In such a case, the actual size of the discrete spectral support of object field (s_o) is calculated in the multiples of Fourier spectral pixels and expressed without physical units as

$$s_O = \frac{N \cdot p}{M} \frac{\mathrm{NA}}{\alpha \cdot \lambda}, \quad (2)$$

where p is the pixel size, NA stands for the numerical aperture of the optical system, M is the magnification, λ is the wavelength, and α is the prefactor of the resolution limit definition ($\alpha = 0.5$ for Abbe's definition).

The limit, $s_o^{\max}$, can be relaxed up to the level of $N/2$ by nonlinear filtering techniques instead of the Fourier

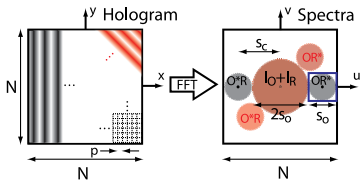

Fig. 1. (Color online) (Left) Off-axis hologram and (right) its spectrum are depicted with the tilt of reference wave field on x axis (gray) or in diagonal (red), where I_O and I_R are the intensities, s_o is the size of the discrete Fourier spectral support of the object field, and N is the count of p-sized pixels.

filtering [7]. In either case, once the object complex field is spatially filtered, keeping the N^2 sampling for further processing (e.g., Fresnel propagation) brings redundant computational burden due to the oversampled nature of the complex field. Hence, it is here proposed to downsample the complex field down to the size of the discrete support of s_o simply by cropping in the Fourier spectral domain and speeding up the following steps of reconstruction. The proposed approach however reduces the field of view slightly in case of aperture apodization with fixed pixel count against border artifacts [8].

The theoretical speed-up factor reaches to 3.4× for a reconstruction scenario involving the complex field decoding and Fresnel approximation propagation. Complex field decoding starts with a 2D fast Fourier transform (FFT) of an N^2 hologram. The resulting spectrum is first cropped to $(N/4)^2$ around one interference term, and values outside the circular bandwidth are set to zero. The complex field is then recovered by a 2D inverse FFT (IFFT) of this cropped and filtered spectrum with the size of $(N/4)^2$. Finally, two consecutive 2D FFTs are applied for propagation on $(N/4)^2$ complex field after a numerical lens correction [9] with the propagation kernel multiplication in between them. The speed-up factor estimation of 3.4× is based on these four 2D FFT stages, each having the computational complexity of $O(M^2 \log M)$ for an M^2-sized array ignoring intermediate multiplication steps.

The performance gain is even more dramatic for an application involving the AF of the complex field by iterative digital propagation. The processing steps involved in a typical AF methodology are illustrated in Fig. 2. The

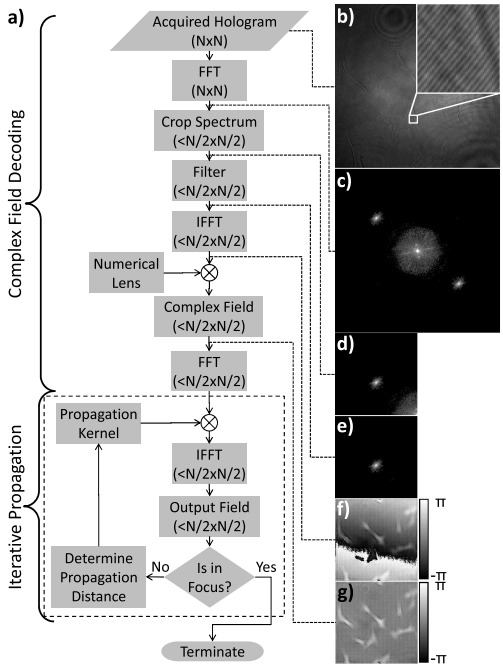

Fig. 2. (a) Block diagram illustrating the steps involved for AF with two subsections of complex field decoding and iterative propagation. Exemplary images (b)–(g) are given for an experimental hologram at the output of every step in complex field decoding: (b) acquired hologram, (c) its log scale spectrum, (d) cropped spectrum, (e) filtered and cropped spectrum, and phase map in hologram plane (prior to propagation) (f) before and (g) after numerical lens.

flow chart of Fig. 2(a) shows the individual steps of AF, and intermediate outputs are depicted in Figs. 2(b)–2(g). Depending on the choice of the focus criterion, the number of iterations to reach the focused field may vary, but the performance gain will be similar at different scales due to reduced size of matrices on which multiple 2D FFTs are applied. Hereafter, the variance of the complex field amplitude is considered as the focus criterion, as it reaches its minimum monotonously as the propagation distance approaches to focus for the objects with minimal amplitude variation like mammalian cells [6,10]. For a more generalized approach that works on various types of objects, another AF method exploiting the wavelength dependence of diffraction in multiwavelength holograms [11] can be employed. Accordingly, propagation distance is determined by Brent's method in which golden section search or parabola fitting is used to calculate the propagation distance for the next iteration step [12]. This specific AF methodology is implemented in LabVIEW, and the average runtimes on a workstation PC (Intel Core 2 Duo E8400 CPU at 3.00 GHz, 3.25 GB RAM, Windows XP 32 bits, NI LabVIEW 7.1) are given in Table 1 for the steps shown in Fig. 2. In all cases, iterative propagation typically convergences after 14 propagation cycles [a propagation cycle is indicated in Fig. 2(a) by the dashed box]. As one can expect, most of the computational load is linked to the iterative Fresnel propagation for uncropped holograms, and its weight in the total load decreases with the resampling factor and approaches balance with complex field decoding. For the both hologram sizes (1024^2 and 512^2) given in Table 1, approximately 4× and 12× faster focusing is achieved for sampling sizes of $(N/2)^2$ and $(N/4)^2$. Besides, AF times of around 50 ms for 512^2 holograms cropped to 128^2 enable real-time AF provided that the acquisition is fast enough.

This possibility of real-time operation finds an interesting application for multimodal imagers employing off-axis DH along with another imaging modality functioning strictly in focus, like fluorescence microscopy. In such a system, common approach is to visit different sample distances and evaluate the focus iteratively until the convergence in the optimal distance. Such an approach requires many acquisitions to converge, resulting in slow frame rates, and it may entirely fail under dynamic conditions. Furthermore, multiple sample acquisitions may be an issue under tight power budgets and for sensitive samples expressing degradation under light exposure. This situation renders dual-mode DH and fluorescence microscopy for live cell imaging as a suitable application case. Earlier it was proposed and patented to numerically sharpen out-of-focus fluorescence images with the aid of complex field attained from the DHM mode [13]. Indeed, in order to avoid photobleaching or phototoxicity, it is desired to minimize the excitation light exposure of the cells during fluorescence imaging.

A dual-mode microscope can exploit the AF in DHM mode by feeding the corresponding autofocus distance in object space to a motorized stage controlling the axial object position and thus keep the fluorescence microscopy images in focus. The critical elements of this microscope are illustrated in Fig. 3(a) where object O and reference R beams of the DHM mode are shown. These beams are combined at the filter cube acting as a beam

Table 1. Computational Performance Comparison of AF with and without Spectral Cropping

Hologram Size (N^2)	Sampling Size	AF Time (ms)	Computation Load (%)	
			Complex Field Decoding	Iterative Fresnel Propagation
1024^2	Full	2861	16.5	83.5
	$(N/2)^2$	709	29.9	70.1
	$(N/4)^2$	223	39.9	60.1
512^2	Full	642	13.8	86.1
	$(N/2)^2$	160	25.4	74.6
	$(N/4)^2$	54	41.8	58.2

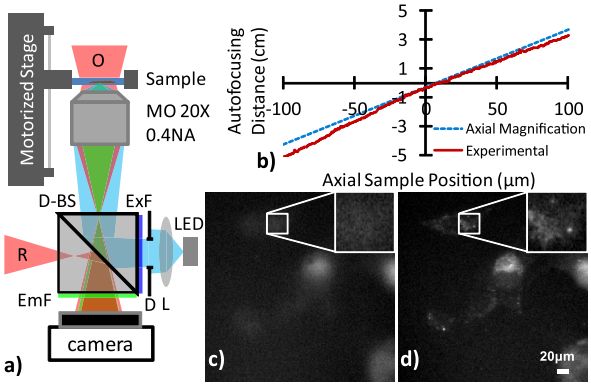

Fig. 3. (Color online) (a) Schematic illustrating the critical elements in the DH-epifluorescence dual-mode microscope. The filter cube includes a dichroic beam splitter (D-BS) ($\lambda_{\text{cut-off}}^{\text{D-BS}} = 500$ nm) along with the short pass excitation (ExF) ($\lambda_{\text{cut-off}}^{\text{ExF}} = 500$ nm) and long pass emission (EmF) ($\lambda_{\text{cut-off}}^{\text{EmF}} = 500$ nm) filters. (b) Axial sample position and DHM mode AF distance relation for experimental calibration (solid red) and the approximation by axial magnification (dashed blue). (c), (d) Live cell fluorescence imaging (c) without and (d) with DHM-fed refocusing.

splitter (85/15, $\%T/\%R$) in this mode, and resulting holograms are recorded by the CCD camera. An LED ($\lambda_{\text{center}} = 470$ nm, $\Delta\lambda = 30$ nm) serves as the excitation source in the epifluorescence microscopy mode. The excitation beam is shaped by a lens L and diaphragm D and directed onto the sample by the filter cube through the 20×, 0.4 NA MO. Fluorescence emission from the sample is imaged on the camera by the MO. Since a single camera is shared for both operation modes, individual modes are time sequentially operated. Position of the imaged sample is controlled by a motorized stage.

The propagation distance of the autofocused hologram is an image space distance, so the object space quantity is required to move the motorized stage. One can choose the axial magnification of the imaging system (M^2) for distances up to few multiples of depth of field (DOF) from the nominal imaging condition [14]. A more appropriate approach is to go through a calibration procedure in which sample position is changed by known increments, for which AF distance is evaluated each time. Figure 3(b) shows the relation between axial sample position and AF distance for the MO in use. The dashed blue curve shows the calculated linear relation between them using the axial magnification, while the output from the calibration procedure is plotted in solid red. As shown by the graph, the larger the distances, the larger the mismatch between the two. In this specific case, this mismatch reaches to a unit multiple of the DOF for an object seven times the DOF away from the object plane. Hence, the calibration data are used for a better performance in the following. Practically, a fourth-order polynomial is fitted to the calibration data once, and this polynomial is used to look up the object space distances corresponding to AF distances retrieved in the DHM mode. During operation, after each DHM acquisition, the motorized stage is moved by an amount cancelling the calculated object space distance. In such a way, the sample is always kept in focus prior to the epifluorescence microscopy acquisition. Exemplary fluorescence images of live mouse myoblast cells with Fluo-4 labeling are shown in Figs. 3(c) and 3(d). Figure 3(c) shows an out-of-focus image, and the subsequent fluorescence image is shown in Fig. 3(d) before which a single DHM image was acquired and automatically followed by a physical focus following the procedure above.

In conclusion, we demonstrated digital off-axis hologram AF performance approaching real time by critical sampling of the complex field. The presented method is typically put into use for a DH-fluorescence dual-mode microscope with single-shot physical AF, dedicated to live cell imaging in the challenging environment of an aircraft performing parabolic flights for microgravity experiments.

The authors thank the EPFL Space Research Programme (ESRP) for the financial support, European Space Agency (ESA) for the PRODEX program financial support, Novespace and ESA for the parabolic flights, and Lyncée tec (www.lynceetec.com) for the technical help.

References

1. J. W. Goodman and R. W. Lawrence, Appl. Phys. Lett. **11**, 77 (1967).
2. D. Gabor, Nature **161**, 777 (1948).
3. E. Leith and J. Upatnieks, J. Opt. Soc. Am. **52**, 1123 (1962).
4. P. Marquet, B. Rappaz, P. Magistretti, E. Cuche, Y. Emery, T. Colomb, and C. Depeursinge, Opt. Lett. **30**, 468 (2005).
5. N. Pavillon, A. Benke, D. Boss, C. Moratal, J. Kühn, P. Jourdain, C. Depeursinge, P. J. Magistretti, and P. Marquet, J. Biophotonics **3**, 432 (2010).
6. M. Toy, S. Richard, J. Kühn, A. Franco-Obregón, M. Egli, and C. Depeursinge, Biomed. Opt. Express **3**, 313 (2012).
7. N. Pavillon, C. Seelamantula, J. Kühn, M. Unser, and C. Depeursinge, Appl. Opt. **48**, H186 (2009).
8. E. Cuche, P. Marquet, and C. Depeursinge, Opt. Commun. **182**, 59 (2000).
9. T. Colomb, E. Cuche, F. Charrière, J. Kühn, N. Aspert, F. Montfort, P. Marquet, and C. Depeursinge, Appl. Opt. **45**, 851 (2006).
10. P. Langehanenberg, B. Kemper, D. Dirksen, and G. von Bally, Appl. Opt. **47**, D176 (2008).
11. P. Gao, B. Yao, R. Rupp, J. Min, R. Guo, B. Ma, J. Zheng, M. Lei, S. Yan, D. Dan, and T. Ye, Opt. Lett. **37**, 1172 (2012).
12. R. P. Brent, *Algorithms for Minimization without Derivatives* (Prentice-Hall, 1973).
13. F. Dubois and C. Yourassowsky, "Method and device for obtaining a sample with three-dimensional microscopy," U.S. patent 7,009,700 (7 March 2006).
14. E. Shaffer, P. Marquet, and C. Depeursinge, Opt. Express **18**, 17392 (2010).